ISSN 1063-7796, Physics of Particles and Nuclei, 2020, Vol. 51, No. 3, pp. 258–262. © Pleiades Publishing, Ltd., 2020.

Femtoscopic Structure of Relativistic Heavy Ion Collisions in the Integrated HydroKinetic Model

Yu. M. Sinyukov[a, b], *, M. D. Adzhymambetov[a], **, V. M. Shapoval[a], *, and V. Yu. Naboka[a], ******

[a] *Bogolyubov Institute for Theoretical Physics, Kiev, 03143 Ukraine*

[b] *Tomsk State University, Department of Physics, Tomsk, 634050 Russia*

**e-mail: sinyukov@bitp.kiev.ua*

***e-mail: adzhymambetov@gmail.com*

****e-mail: shapoval@bitp.kiev.ua*

*****e-mail: nvlad1@ukr.net*

Received September 20, 2019; revised October 28, 2019; accepted November 10, 2019

Abstract—The theoretical description of the femtoscopy scales in ultrarelativistic heavy-ion collisions at different energies and for different colliding ion pairs (Au + Au collisions at the top RHIC energy $\sqrt{s_{NN}} = 200$ GeV, Pb + Pb collisions at the LHC energies $\sqrt{s_{NN}} = 2.76$ and $\sqrt{s_{NN}} = 5.02$ TeV, the LHC Xe + Xe collisions at $\sqrt{s_{NN}} = 5.44$ TeV) is provided within the integrated HydroKinetic model (iHKM). The comparison of the model simulation results, obtained for the considered collision types at the similar values of the mean charged particle multiplicity $\langle dN_{\mathrm{ch}}/d\eta\rangle$ shows that the magnitudes of the corresponding interferometry radii depend not only on $\langle dN_{\mathrm{ch}}/d\eta\rangle$, but also on the geometric sizes of the colliding nuclei.

DOI: 10.1134/S1063779620030260

1. INTRODUCTION

The correlation femtoscopy technique [1–3] is a powerful and indispensable tool for the investigation of the space-time structure of the extremely hot and dense systems formed in high-energy nuclear collisions. The method exploits the quantum statistics (Bose–Einstein and Fermi–Dirac) correlations, arising between particles produced in the collision. As it was shown [4–8], the interferometry radii, extracted from the Gaussian fits to the measured two-particle momentum correlation functions of identical particles in heavy ion collisions do not express the total size of the system because its expansion. In [7, 8] it was proposed the general interpretation of the radii as the homogeneity lengths of the system in different directions, i.e. with the scales, at which the corresponding distribution functions $f(x, p)$ do not change much, not more than in 2 times. The femtoscopy radii, related to essentially different particle pair momenta $\mathbf{k}$, characterize different parts of the analyzed system. The reason is that particles are radiated from system's different regions where different local collective velocities are close to velocity of pair with the momenta near $\mathbf{k}$, and these emission regions have different gradients of velocity and temperature—different homogeneity lengths.

On practice, in order to extract the necessary information, one also has to separate "useful" quantum statistics correlations from those caused by the final state interactions (FSI) between produced particles and to take into account the effect of long-lived resonances' decays, which also make contribution to the observed correlation function [9]. In case of baryon-baryon correlation functions, the FSI analysis allows also to extract the quantities characterizing the strong interaction between the corresponding baryons (scattering length, effective range, etc.), including cases, when such extraction is impossible in usual scattering experiments due to insufficient beam densities [10, 11].

Additional information about the space-time picture of a heavy-ion collision can be obtained using the source imaging method [12–14], which allows one to restore the emission source function (i.e., the distribution of the distance between the points of particle emission in the pair rest frame (PRF) integrated over time) from the experimental correlation function. While the standard correlation femtoscopy approach assumes the emission function to be Gaussian, the source imaging reveals the actual shape of source function, which often deviates from the Gaussian one (e.g. the source function can have power-law "tails" in certain directions [15]). Analyzing the extracted source functions, one can better understand the dynamics of the collision process and investigate the role of various effects (particle rescatterings at the late "afterburner" stage of the collision, decays of long-

Table 1. The iHKM main parameters: relative contribution to initial energy density from binary collision α and maximal initial energy density ϵ_0 used to describe different relativistic heavy-ion collision experiments. The initial proper time in all cases is $\tau_0 = 0.1$ fm/c. The simulated events of different centrality, shown in the second column, were selected for the analysis to ensure close charged particle multiplicity $dN_{\text{ch}}/d\eta$ at $|\eta| < 0.5$ values for all types of collision. The first three simulations use Laine–Schroeder equation of state for quark-gluon matter [22], while for the Xe + Xe collisions the HotQCD Collaboratios EoS was applied [23].

Experiment	Centrality, %	$\langle dN_{\text{ch}}/d\eta \rangle$	α	ϵ_0, GeV/fm^3	EoS
Au+Au @ 200 GeV	0–5	688	0.18	235	L.-S.
Pb+Pb @ 2.76 TeV	19–28	693	0.24	679	L.-S.
Pb+Pb @ 5.02 TeV	23–33	677	0.24	1067	L.-S.
Xe+Xe @ 5.44 TeV	10–19	680	0.44	445	hQCD

lived resonances, space-momentum correlations, etc.) in the formation of final spatiotemporal emission structure.

In order to perform a thorough study and get a reliable interpretation of the measured experimental data on femtoscopy, one will most likely need to simulate the considered collision process in a realistic model and obtain the model description of the corresponding observables. The integrated hydrokinetic model (iHKM) [16] allowed to achieve a successful description of all main bulk observables (particle yields and particle number ratios, p_T spectra, v_n coefficients, interferometry radii) for high-energy Au + Au collisions at the top RHIC energy and Pb + Pb collisions at the two LHC energies [17–19]. In the present work we discuss the theoretical results on the correlation femtoscopy obtained in iHKM for these experiments together with our new results for $\sqrt{s_{NN}} = 5.44$ TeV Xe + Xe collisions at the LHC.

2. RESULTS AND DISCUSSION

The integrated hydrokinetic model simulates the full process of the evolution of hot and dense matter, formed in relativistic nuclear collision. This process can be considered as passing in several successive stages, each described within the model using the corresponding approach. The first simulation stage represents the prethermal dynamics of the system just after the collision in terms of an energy-momentum transport approach in the relaxation time approximation. During this stage the system gradually thermalizes and eventually comes to a state of local chemical and thermal equilibrium, which can be further described in hydrodynamical approach. At the second stage of matter evolution the system undergoes hydrodynamical expansion and behaves as a continuous medium. This stage is simulated within Israel–Stewart relativistic viscous hydrodynamics formalism.

In course of time the system loses local equilibrium and decouples into particles—we call this "particlization" stage of the evolution. At the particlization hypersurface, assumed to be an isotherm of temperature T, close to 160 MeV and depending on the equation of state (EoS) for quark-gluon matter, utilized at the hydrodynamical stage, a set of particles of various species with their space-time coordinates and 4-momenta are generated according to distribution functions defined at previous stage. Finally, the created particles pass the "afterburner" stage of the system's evolution, when they intensively collide with each other (elastically and inelastically) and the resonances decay. In iHKM this stage is simulated using the UrQMD model [20].

The initial energy-density profile for the first, prethermal stage is generated using the Monte Carlo Glauber approach with the help of GLISSANDO code [21]. The main iHKM parameters are $\epsilon_0(\tau_0)$—the initial maximal energy density at starting proper time τ_0, and α—the parameter, regulating the proportion between the "binary collisions" and the "wounded nucleons" models' contributions to the GLISSANDO-generated distribution. These parameters are fixed for each collision type based on the experimental data as giving the best fit to the measured dependence of charged particle multiplicity on collision centrality and the slope of pion spectrum in central events.

In [17–19] the iHKM parameters were adjusted for the description of RHIC Au + Au collisions at $200A$ GeV and the LHC Pb + Pb collisions at $2.76A$ and $5.02A$ TeV. Among other results, a description/prediction of the femtoscopy radii was obtained. Recently iHKM was also tuned to describe the Xe + Xe collisions at the LHC energy $5.44A$ TeV (see the utilized model parameter values in Table 1). In this work we decided to compare the obtained radii values, as well as the corresponding interferometry volume values in events with the same multiplicity in order to answer the question: do the interferometry scales depend almost linearly only on the mean charged particle density ("scaling hypothesis"), as it is often claimed in the studies devoted to correlation femtoscopy (see, e.g. [24]), or not, and apart from the multiplicity, geometrical sizes of the colliding nuclei also have to be taken into account, as it was concluded in the previous papers by our research group [25, 26], see Fig. 1.

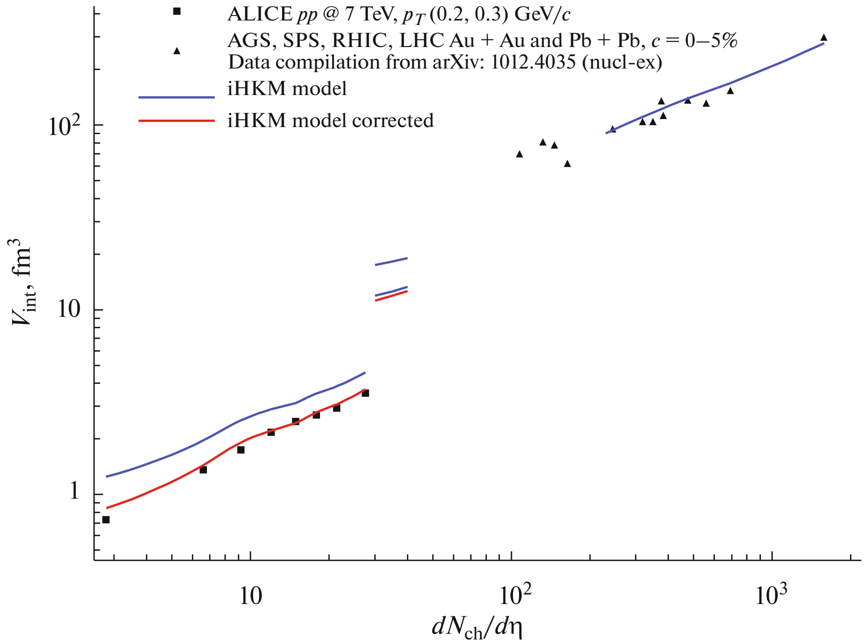

Fig. 1. The interferometry volume $V_{int} = R_{out}R_{side}R_{long}$ dependency on the charged particle multiplicity $dN_{ch}/d\eta$. The lines at the left demonstrate the iHKM results for $p + p$ collisions at the LHC energy $\sqrt{s}$ = 7 TeV, while the lines at the right correspond to different central $A + A$ collisions. The model points are compared to the experimental data related to AGS, SPS, RHIC and LHC [27–35]. The dark curves represent raw model results, and the light curves correspond to the results with the quantum corrections applied according to [26]. The line segments in the middle show the model predictions for the p + Pb LHC collisions at $\sqrt{s}$ = 5.02 TeV calculated using the two initial transverse system sizes—R = 1.5 fm (upper line) and R = 0.9 fm (lower lines).

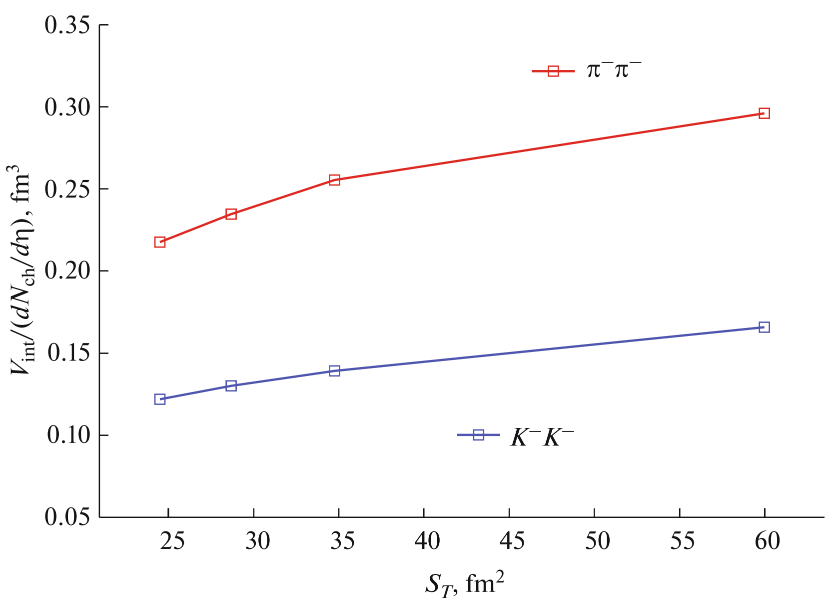

Fig. 2. The iHKM results on pion and kaon interferometry volume $V_{int} = R_{out}R_{side}R_{long}$ divided by charged particle multiplicity $dN_{ch}/d\eta$ for different collision types, characterized by the initial transverse overlap area of colliding ions S_T. The points from left to right correspond to the following systems: Pb + Pb @ 5.02, Pb + Pb @ 2.76, Xe + Xe @ 5.44 TeV, and Au + Au @ 200 GeV. The collision centralities are listed in Table 1.

In Fig. 2 we show the dependency of pion and kaon interferometry volume $V_{int} = R_{out}R_{side}R_{long}$ on S_T—an effective parameter, characterizing the initial transverse area of the system, formed in relativistic heavy-ion collisions. The value of S_T is calculated for each collision type, presented in Table 1, as the transverse

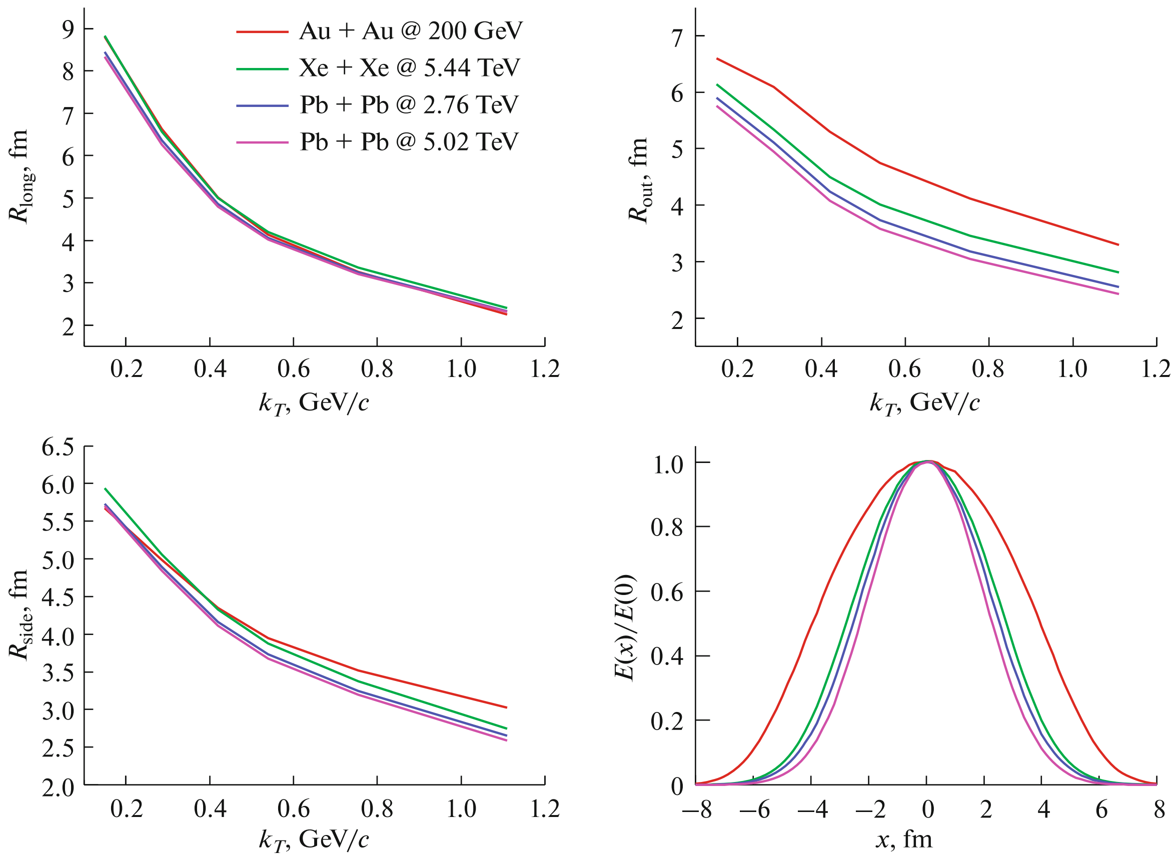

Fig. 3. The iHKM results on kaon femtoscopy radii in different collisions (see Table 1 for details) and the corresponding rescaled initial transverse energy-density profiles $\epsilon(x)/\epsilon_0$.

near elliptic area of initial energy density profile. Thus, $S_T = \pi ab$, where a and b are the semi-axes of the ellipse, formed at half-value of the maximal energy density in the system. The volume values are divided by $\langle dN_{ch}/d\eta \rangle$ to eliminate the influence of small differences between charged particle multiplicity values for different experiments. The femtoscopy radii and volume correspond to the pair transverse momentum $0.2 < k_T < 0.3$ GeV/c. The particles with transverse momenta from the range $0.1 < p_T < 1.55$ GeV/c, and with pseudorapidity from the range $|\eta| < 0.8$ were selected to construct the corresponding correlation functions.

As one can see from the plot, the pion volume values are about 2 times higher, than the kaon ones, and both dependencies are not flat—the volumes grow noticeably with the transverse size of the system. At near the same multiplicities, the size is minimal for the LHC Pb + Pb collisions at 5.02A TeV, for the lower energy 2.76A TeV it is slightly bigger, then follows the size of Xe + Xe collisions at 5.44A TeV, and the maximal S_T value is for Au + Au collisions at the top RHIC energy.

A similar behavior can be noticed in the next plot (Fig. 3), where the dependencies of individual kaon femtoscopy radii R_{out}, R_{side}, and R_{long} on k_T are demonstrated for the four considered collision types. In addition, the plot of rescaled initial transverse energy-density distributions $\epsilon(x)/\epsilon_0$ for all the collision types is shown. From the plots it follows, that the main contribution to the difference between interferometry volumes for different systems comes from the transverse radii: mostly from R_{out} radii, the *side* direction gives smaller contribution. At the same time the *long* radii for all the systems almost coincide. This fact supports the suggestion that the differences between the interferometry volumes originate from the differences in collective transverse flow in the considered systems, which in turn depends on the initial geometrical sizes of the system [25, 26] and corresponding energy/pressure gradient. Table 1 confirms this conclusion.

3. CONCLUSIONS

The iHKM results on femtoscopy scales of relativistic Au + Au collisions at the top RHIC energy, as well as Pb + Pb and Xe + Xe collisions at the LHC energies, in events with similar multiplicities are presented. The interferometry volume and radii dependencies on the effective initial transverse size of the nuclei overlapping region, characterizing the collision, are analyzed. It is shown, that the transverse radii and the volume depend on both the mean charged particle multiplicity and the initial geometrical size of the system, and increase when corresponding values grow.

4. FUNDING

The research was carried out within the scope of the International Research Network "EUREA: European Ultra Relativistic Energies Agreement" and the corresponding Agreement with the National Academy of Sciences (NAS) of Ukraine. The work is partially supported by Tomsk State University Competitiveness Improvement Program.

REFERENCES

1. G. Goldhaber, S. Goldhaber, W. Lee, and A. Pais, Phys. Rev. **120**, 325 (1960).
2. G. I. Kopylov and M. I. Podgoretsky, Sov. J. Nucl. Phys. A **15**, 219 (1972); **18**, 336 (1973); **19**, 215 (1974).
3. G. Cocconi, Phys. Lett. B **49**, 459 (1974).
4. S. Pratt, Phys. Rev. D **33**, 1314 (1986).
5. A. N. Makhlin and Yu. M. Sinyukov, Sov. J. Nucl. Phys. A **46**, 345 (1987); A. N. Makhlin, and Yu. M. Sinyukov, Z. Phys. C: Solid State Phys. **39**, 69 (1988); Yu. M. Sinyukov, Nucl. Phys. A **498**, 151 (1989).
6. Y. Hama and S. S. Padula, Phys. Rev. D **37**, 3237 (1988).
7. Yu. M. Sinyukov, Nucl. Phys. A **566**, 589 (1994); Yu. M. Sinyukov, in *Hot Hadronic Matter: Theory and Experiment,* Ed. by J. Letessier, H. H. Gutbrod, and J. Rafelski (Plenum, New York, 1995), p. 309.
8. Yu. M. Akkelin and Yu. M. Sinyukov, Phys. Lett. B **356**, 525 (1995).
9. Yu. M. Sinyukov, R. Lednický, S. V. Akkelin, J. Pluta, and B. Erazmus, Phys. Lett. B **432**, 248 (1998).
10. R. Lednický and V. L. Lyuboshitz, Sov. J. Nucl. Phys. **35**, 770 (1982); in *Proc. Int. Workshop on Particle Correlations and Interferometry in Nuclear Collisions (CORINNE 90), Nantes, France, 1990,* Ed. by D. Ardouin (World Sci., Singapore, 1990), p. 42; R. Lednicky, J. Phys. G: Nucl. Part. Phys. **35**, 125109 (2008).
11. L. Nemenov, Yad. Fiz. **41**, 980 (1985); V. L. Lyuboshitz, Sov. J. Nucl. Phys. **48**, 956 (1988).
12. D. A. Brown and P. Danielewicz, Phys. Lett. B **398**, 252 (1997).
13. D. A. Brown and P. Danielewicz, Phys. Rev. C **57**, 2474 (1998).
14. D. A. Brown and P. Danielewicz, Phys. Rev. C **64**, 014902 (2001).
15. S. Afanasiev et al. (PHENIX Collab.), Phys. Rev. Lett. **100**, 232301 (2008).
16. V. Yu. Naboka, Iu. A. Karpenko, and Yu. M. Sinyukov, Phys. Rev. C **93**, 024902 (2016); V. Yu. Naboka, S. V. Akkelin, Iu. A. Karpenko, and Yu. M. Sinyukov, Phys. Rev. C **91**, 014906 (2015).
17. M. D. Adzhymambetov, V. M. Shapoval, and Yu. M. Sinyukov, Nucl. Phys. A **987**, 321 (2019).
18. V. Yu. Naboka, Iu. A. Karpenko, and Yu. M. Sinyukov, Phys. Rev. C **93**, 024902 (2016).
19. V. M. Shapoval and Yu. M. Sinyukov, Phys. Rev. C **100**, 044905 (2019); arXiv:1809.07400 [hep-ph].
20. S. A. Bass et al., Prog. Part. Nucl. Phys. **41**, 255 (1998); M. Bleicher et al., J. Phys. G **25**, 1859 (1999).
21. W. Broniowski, M. Rybczynski, and P. Bozek, Comput. Phys. Commun. **180**, 69 (2009).
22. M. Laine and Y. Schroeder, Phys. Rev. D **73**, 085009 (2006).
23. A. Bazarov et al. (HotQCD Collab.), Phys. Rev. D **90**, 094503 (2014).
24. M. Lisa, S. Pratt, R. Soltz, and U. Wiedemann. Ann. Rev. Nucl. Part. Sci. **55**, 357 (2005); M. Lisa, Braz. J. Phys. **37**, 963 (2007).
25. S. V. Akkelin and Yu. M. Sinyukov, Phys. Rev. C **70**, 064901 (2004); S. V. Akkelin and Yu. M. Sinyukov, Phys. Rev. C **73**, 034908 (2006).
26. V. M. Shapoval, P. Braun-Munzinger, Iu. A. Karpenko, and Yu. M. Sinyukov, Phys. Lett. B **725**, 139 (2013).
27. K. Aamodt et al. (ALICE Collab.), Phys. Rev. D **84**, 112004 (2011).
28. K. Aamodt et al. (ALICE Collab.). Phys. Lett. B **696**, 328 (2011).
29. D. Antonczyk, Acta Phys. Polon. B **40**, 1137 (2009).
30. S. V. Afanasiev et al. (NA49 Collab.), Phys. Rev. C **66**, 054902 (2002).
31. C. Alt et al. (NA49 Collab.), Phys. Rev. C **77**, 064908 (2008).
32. J. Adams et al. (STAR Collab.), Phys. Rev. Lett. **92**, 112301 (2004).
33. J. Adams et al. (STAR Collab.), Phys. Rev. C **71**, 044906 (2004).
34. S. S. Adler et al. (PHENIX Collab.), Phys. Rev. C **69**, 034909 (2004).
35. S. S. Adler et al. (PHENIX Collab.), Phys. Rev. Lett. **93**, 152302 (2004).